INVITED PAPER

Transport-Based Biophysical System Models of Cells for Quantitatively Describing Responses to Electric Fields

Computational methods used to describe biological cell system responses to electric fields are reviewed in this paper; such methods are potentially useful for design of electroporation systems.

By Thiruvallur R. Gowrishankar, Kyle C. Smith, and James C. Weaver

ABSTRACT | In this paper, we review computational methods based on spatially distributed transport models that we have used to describe biological cell system responses to electric fields. Application to electroporation (EP) is emphasized, as it is increasingly used experimentally, but is not well understood quantitatively. We argue that Cartesian transport lattices (CTLs) and meshed transport networks (MTNs) are appropriate for describing transport in cellular systems generally. The approach is based on mathematical descriptions of transport in 1-D, which are then assigned to intranodal regions in 1-D, 2-D, and 3-D cell system geometries. Electrical behavior is based on nonspecific charge movement. Descriptions of heat transfer and both molecular and ionic transport have also been examined. This approach allows both traditional, idealized geometries [e.g., cylindrical, spherical plasma membrane (PM)] and also more realistic, irregular cell shapes and sizes to be used approximately, with little difference in computational difficulty. The more complex (active) local membrane models are similar to "agents" in agent-based modeling, in the sense that it is the individual responses of interactions within local regions that yield overall system behavior, which can be emergent and nonintuitive. Cell system models may be useful for screening of EP candidate combinations of pulse parameters, cell characteristics, and molecular transport properties with the goal of optimizing existing experimental protocols and possibly discovering new effects and applications.

KEYWORDS | Distributed transport model; electroporation (EP); meshed transport networks (MTNs); transport lattice

I. INTRODUCTION

The response of living cells to both endogeneous and exogenous electromagnetic fields is of long standing interest. Biologically generated currents are created by metabolically driven ion pumps and electron transport within biomolecules, and have associated endogenous electric fields within and near cells, giving rise to longer ranging natural fields in organized, multicellular systems. Action potentials of excitable cells are extremely important, and well studied by many, so it is not our main focus. Instead, we concentrate on the electroporation (EP) response fields that are created within and near single-cell and multicellular systems due to externally applied fields. Briefly, EP is a mechanistic hypothesis involving electrically assisted formation of transient aqueous pores in the lipid regions of cell membranes [1], [2]. Characteristic pulse durations vary from 1 ns to almost 1 s, with corresponding field strengths of ~100 kV/cm down to 0.1 kV/cm.

Manuscript received September 23, 2011; revised February 27, 2012 and April 24, 2012; accepted May 5, 2012. Date of publication July 16, 2012; date of current version January 16, 2013. This work was supported by the National Institutes of Health under Grant GM063857.

T. R. Gowrishankar and **J. C. Weaver** are with the Harvard-MIT Division of Health Sciences and Technology, Massachusetts Institute of Technology, Cambridge, MA 02139 USA (e-mail: jcw@mit.edu).

K. C. Smith is with the Harvard-MIT Division of Health Sciences and Technology, Massachusetts Institute of Technology, Cambridge, MA 02139 USA and also with the Center for Engineering and Medicine, Massachusetts General Hospital, Boston, MA 02114 USA.

Digital Object Identifier: 10.1109/JPROC.2012.2200289

For single (isolated) mammalian cells the spatial scales of interest range from the molecular level (subnanometer) to the cell membrane level (~5 nm) to a single mammalian cell level (~10 μm). For multicellular systems (tissue level) there is a wide range of sizes, starting with models that explicitly treat a few, distinguishable individual cells (idealized or irregular geometry; ~100 μm). For larger numbers of cells there is often a leap to ~1 mm, with a continuum approximation that is based on bulk tissue properties. Finally, there is increasing development and use of anatomically correct partial- and whole-body models (~1 mm to ~1 m) that are constructed from different tissue-level models. Looking forward, it should soon be possible to begin combining models at these different levels.

Both Cartesian transport lattices (CTLs) and meshed transport networks (MTNs) offer the potential benefit and burden of creating irregular membrane geometries to which specific functional responses can be assigned. One can thus go beyond traditional spherical and spheroidal geometries. Further, local membrane properties can range from spatially distributed voltage-gated ion channels to local membrane lipid composition that affects electroporation. Such extensions are motivated by irregularly shaped organelles (endoplasmic reticulum, mitochondria). However, such models do not have geometric symmetries or other simplifications that can be exploited to reduced computational demands. Instead, both geometric and local model attributes will generally increase computational requirements. As computational power increases it may therefore be desirable to pursue addition of these types of increased biological realism to cell system models.

II. GENERAL APPROACH

We describe electrical behavior by considering the movement of nonspecific, nonquantized electrical charge, in the spirit of classical continuum electrodynamics. Small ions (Na^+, K^+, and Cl^-) are in normal physiologic aqueous media at total concentrations of 0.2–0.3 M. These dominate bulk media electrical conductivity, even within the overcrowded cytoplasm where there is a fourfold reduction in diffusion coefficients (and electrical mobilities) [3].

In most cases, the net (cumulative) charge transport associated with a cell due to an external electric field exposure involves a very large number of small ions. Thus, averaging occurs. Accordingly, we use the continuum approximation in which the stochastic behavior of individual ions is usually unimportant. A basic consequence is that we can use deterministic electrical circuit descriptions to construct cell system models.

In this general approach, quantitative, approximate descriptions of cellular systems and their electrical behavior are obtained by computing the response electric field (and, if needed, the associated current density $\vec{J}$). Typically the applied field is uniform, meaning that if no cell were present, the equipotentials would be parallel and evenly spaced, with $\vec{E}_{\rm app} = \vec{J}/\sigma_{\rm e}$, perpendicular to the equipotentials. Here $\sigma_{\rm e}$ is the electrolyte conductivity, assumed fixed. The response field is the redistributed field in the presence of cells and interactions such as EP that significantly change membrane electrical properties. These changes are generally spatially heterogeneous and often change rapidly with time.

Our illustrations emphasize cell EP [1], [4]. In this case, there are rapid, large changes in local cell membrane

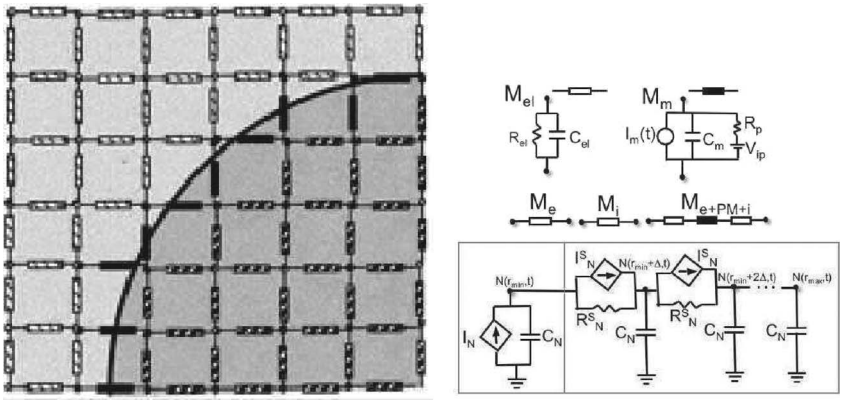

Fig. 1. *Left: Part of the transport lattice that represents the interface between a membrane and two electrolytes. The charge transport and storage models that interconnect adjacent Cartesian nodes are shown as rectangles. Right: CTL equivalent circuits for models of electrolyte and dynamic EP [21], [32]. These represent functional local models of electrolyte* (M_e)*, membrane* (M_m)*, and the PM-electrolyte interface* (M_{e+PM+i})*, in a 101* $\times$ *101 CTL; the lattice spacing,* ℓ*, as well as the depth of the system model, is 1* μ*m, leading to a spatial scale of 100* μ*m* $\times$ *100* μ*m. The equivalent EP circuit representing the asymptotic membrane EP model [17] (left gray box) and its extension to the dynamic (expanding and contracting pores) membrane EP model with pore expansion/contraction described by the Smoluchowski equation (SE; right gray box) [32] is assigned to each local membrane site. The resulting local pore distributions are discretized, with drift and diffusion in pore radius space. A non-Ohmic pore conductance* G_m *that is input for the time-dependent membrane current* $I_m(t)$ *is used in* M_m*. Note that "m" is a general label for membranes; "PM" shown here is for the outer plasma membrane.*

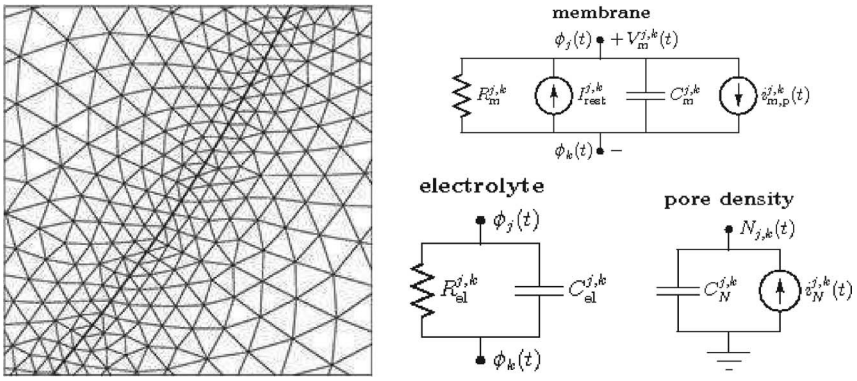

Fig. 2. *Left: Enlarged region of an MTN model shown in Fig. 7. The density of nodes is higher in the proximity of the membrane. Right: MTN local model equivalent subcircuits [34] for Fig. 7. An electrolyte or membrane subcircuit is located between each pair of adjacent nodes in the cell system. The electrical transport is determined by the local mesh geometry, passive electrical properties of the electrolyte and membranes, and, at the membranes, by the instantaneous pore density and associated time-dependent conductance, which provide a rapidly changing (active) response mechanism. In the cell system model, each membrane subcircuit has an associated pore density (units: m^{-2}) subcircuit that is used to calculate pore accumulation. In a passive model, there are no pores, and the membrane conductance is constant.*

conductance that depends on both membrane site and time. Both the creation and evolution of dynamic, heterogenous pore populations and simultaneous redistribution of fields and transmembrane voltages including memory effects (hysteresis) can therefore be complicated.

We have developed and solved two types of transport-based models: CTLs and MTNs. In CTLs, the system geometry (membranes and electrolytes) is described on a Cartesian lattice with regularly spaced lattice points. The membranes generally lie in regions between lattice points (Fig. 1). The regions between lattice points are assigned local charge transport or charge storage models that include nonlinear representation of the local ion channel population and membrane electroporation [5]. In contrast, MTNs have variable mesh element size based on the system geometry. For example, small elements are near the membrane and larger elements are away from the membrane (Fig. 2). In MTNs, a triangular mesh of the system is generated, and Voronoi cells (VCs) that enclose all points in space closer to a given node than to any other are identified [6].

III. MODELING EXAMPLES

Both CTLs and MTNs have been used to study single- and multiple-cell responses to electric fields. We initially approximated cell geometries by using CTLs that respected topology but often only roughly respected cell morphology, whether traditional idealized shapes (cylinders and spheres) or irregular geometries, particularly multiple cells close together (typical of in vivo environments). Usually we created and solved 2-D models. Although 3-D models can be created, their solution is much more computationally demanding, and the main features of cells appear to lie more with the topology and approximate size of cell membranes than 3-D models. CTLs for 3-D cells are included in our examples, and have been created and solved with EP (Gowrishankar *et al.*, unpublished), but have not yet approached the level of membrane detail and dynamic treatment of heterogeneous, transient pore populations that are possible in 2-D. MTNs were employed later, to more faithfully represent cell geometries while simultaneously improving computational efficiency [7], [8]. Here we present examples of systems modeled using CTL and MTN methods.

A. CTLs With Passive Membranes

Our initial models used CTLs nodes in 2-D and 3-D. This allowed exploration of potential uses and partial validations for versions of traditional single-cell models (spherical and cylindrical PMs). Accordingly, we first showed that a discretized approximation to a passive spherical membrane yields frequency-domain results [5] which were in good agreement with analysis by traditional analytical methods [9] (Fig. 3).

A passive membrane has fixed conductive and dielectric properties, and is appropriate for exposures with small applied field magnitudes. The spherical plasma membrane (PM) is coarsely discretized. Computational constraints led us to using a small (aqueous electrolyte-filled) simulation box [5]. This means that the usual analytic condition of infinitely distant field sources is not applicable. Nevertheless, quantitative comparison of the frequency-domain solutions showed only minor differences compared to a traditional model construction and solution [9] in the frequency-dependent amplifcation [gain $G_m(f)$] of the membrane (Fig. 3), by which it is meant that the high resistance concentrates (amplifies) fields across the thin PM. The low-frequency transmembrane voltage change at the sphere's poles for a high resistivity membrane is

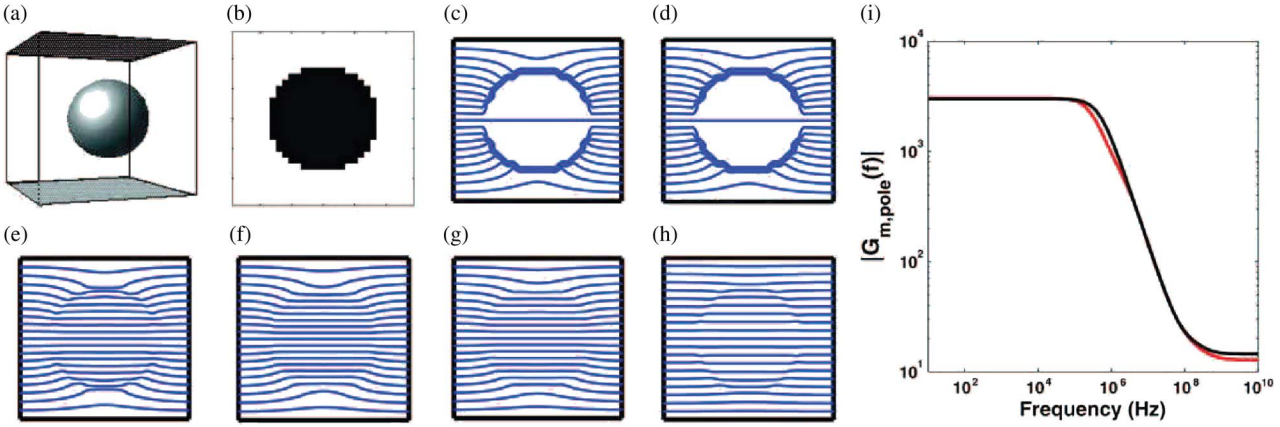

Fig. 3. *Frequency response of a descretized spherical cell model and a partial validation of CTLs [5]. Spherical cell model (r_{cell} =10 μm) for nearly insulating membrane resistivities [5]. (a) Perspective drawing with ideal parallel plane electrodes (top black and bottom gray) that provide an applied electric field E_{app}. (b) Approximation of spherical cell (cross section). (e)–(h) Equipotentials (blue) for membrane resistivity $\rho_m = 10^8$ m, and f = 100 Hz, 100 kHz, 1 MHz, 10 MHz, 100 MHz, and 1 GHz, respectively. (i) Magnitude of the frequency-dependent membrane field gain at the cell's poles $G_{m,pole}(f)$ predicted by the CTL model (red) and by a second-order analytic model (black) [9].*

0.99 of the analytic results. Subsequently, a 2-D (cylindrical or circular PM) model provided additional partial validation in the time domain [10]. Traditional analytic solutions were compared with numerical results from a discretized circular passive PM, and were in close agreement.

In view of increased interest in EP with microfluidics, we modeled a spatially heterogeneous applied field with the same 3-D discretized spherical cell. In this case, one planar electrode was replaced with a discretized short, needle-like electrode [11]. The electrical response in the frequency domain showed that as the frequency was increased the cell's presence caused progressively less response field heterogeneity (due to decreased impedance of the passive PM). If extended to the time domain, such models may be relevant to the increased use of elongated, narrow electrodes of varying size to cause EP [12], [13].

In vivo environments of humans and other multicellular organisms are much more complex than isolated cells. Therefore, the single-cell CTL models were extended to multicellular systems [5]. As shown in Fig. 4, a didactic multicellular model was constructed, motivated by the existence of multicellular systems near organs. Accordingly, the multicellular model featured three regions: 1) a relatively simple invagination containing an aqueous medium (physiologic electrolyte); 2) an endothelial monolayer of cells connected by tight junctions, but with (purposefully) a defect present, which partially compromised the monolayers' barrier function; and 3) ~50 elongated, irregular subendothelial cells. The frequency response of the multicellular system to low magnitude fields showed the current density was concentrated within the cell layer gap, but this concentration diminished with increasing frequency beyond 300 MHz.

B. CTL With Asymptotic Membrane EP Model

In 1999, others introduced a cell EP model by combining traditional analytic approaches of a spherical cell [14], [15] with the asymptotic membrane electroporation model [16]. This was an important advance. These first two papers demonstrated cell models with important characteristic behavior of spatially and temporally distributed EP electrical behavior, including a significant flattening of the transmembrane voltage and pore density (pores per area) response as a function of location (angle from the cell's two poles). The asymptotic membrane EP model considers only two states: 1) no pore or 2) a pore of fixed radius, usually r_{min} = 0.76 nm (now often rounded up to 0.8 nm) [14]–[16]. The large number of pores created by a sufficiently large electrical pulse causes a shunting of the membrane current, limiting the transmembrane voltage to ~1 V.

In 2004, system models of a 2-D CTL circular cell and a budding (mother/daughter) yeast cell pair were described [17]. Both used CTLs for nonspecific charge movement, a resting potential source and the asymptotic membrane EP model. It introduced the term supra-electroporation, and showed that without the creation of a very large number of conducting pores the transmembrane voltage would become implausibly large (e.g., ~30 V). The immense number of pores greatly increased membrane conductance, preventing a large transmembrane voltage. The extracellular and intracellular electric fields then become essentially the same.

In 2006, the CTL approach was used to construct and solve a single (isolated) cell model with both the traditional outer PM and also several internal organelle membranes [18]. These included a nucleus with double membranes (NM), four mitochondria with double

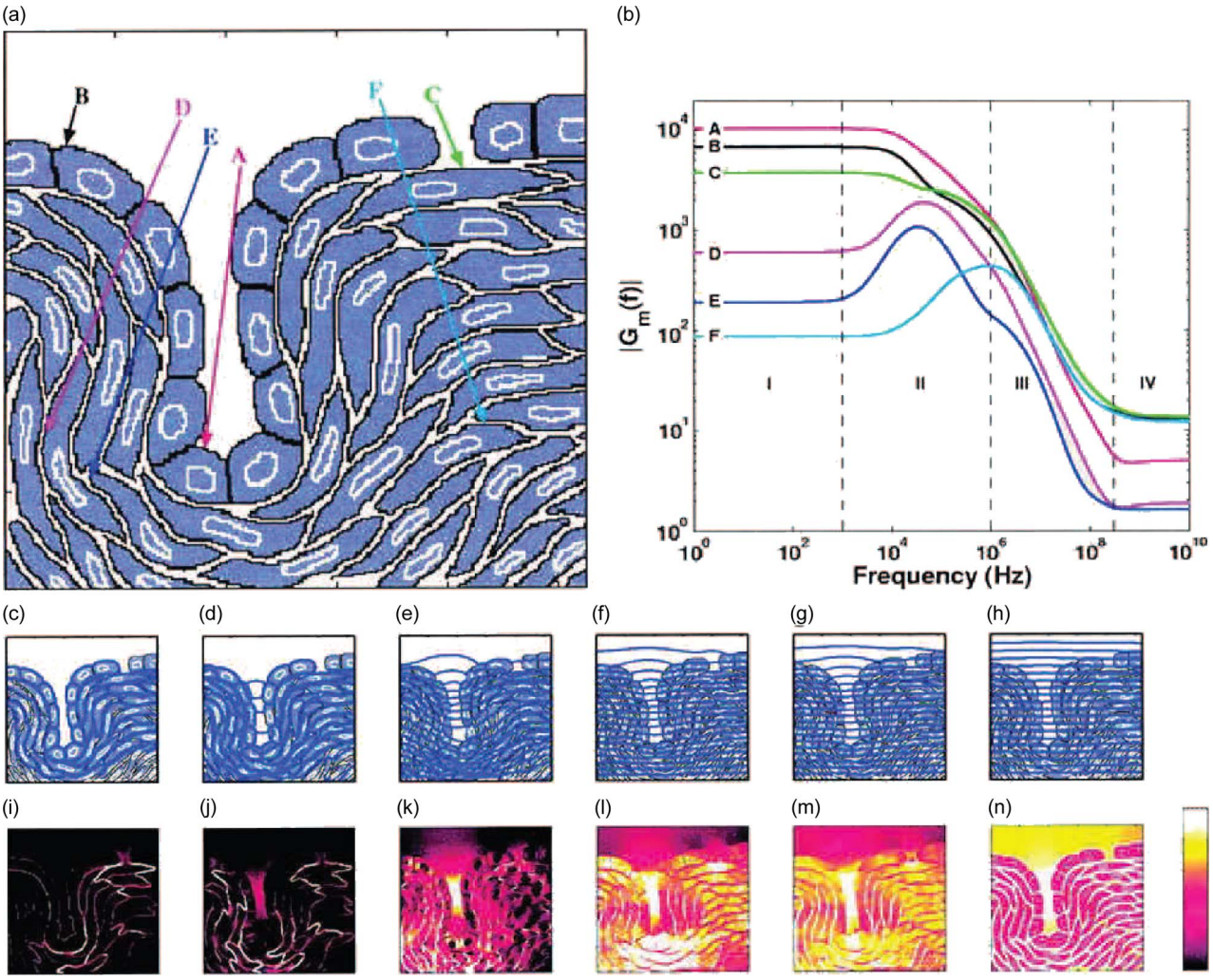

Fig. 4. *Didactic multicellular system model [5]. (a) Electrolyte-filled cavity and endothelial layer with cells connected by tight junctions, with an invagination and a gap in the cell layer. The upper region is saline (extracellular electrolyte). The underlying region contains subendothelial cells with ~15% extracellular field. (b) $G_m(f)$ (field amplification by voltage concentration at membranes [4], [9]) from 10 Hz to 10 GHz at cell membrane sites A–F. Note the emergent behavior for some cells between 1 kHz and about 1 MHz, wherein the partical shielding by some cells results in larger gain for sites at other cells. (c)–(h) Equipotentials for 100 Hz, 100 kHz, 1 MHz, 10 MHz, 100 MHz, and 1 GHz, respectively. (i)–(n) SAR distributions (spatially averaged value of 1 W kg^{-1}; color bar: black = 0 to white ≥ 2 W · kg^{-1}) for the same frequencies. Specific absorption rate (SAR) is proportional to ρJ^2 and is displayed instead of $\bar{J}$ because SAR is more closely related to local heating and possible thermal effects, and is widely used in safety standards. For both the equipotentials and SAR note the concentration within the invagination, which is an example of amplification by current density concentration. Initially, we used circuit analysis (mainly by SPICE), which is fairly general, because many important differential equations can be solved by equivalent circuits [44].*

membranes [mitochondrial outer membrane (MOM); mitochondiral inner membrane (MIM)] and an endoplasmic reticulum with a single membrane (ER). Each of these membranes had a resting potential source that yielded a resting potential representative for the particular organelle [18]–[21]. The membranes were assigned the asymptotic EP model (left rectangle in Fig. 1). This cell system model showed that progressively smaller organelles (endoplasmic reticulum, nucleus, mitochondria) were electroporated by nanosecond pulsed electric fields (nsPEFs) as pulse magnitude was increased to $>$ 20 kV/cm (Fig. 5) [18]. This provides a partial explanation of the experimental reports of single-to-multiple submicrosecond, megavolt per meter pulses causing intracellular effects [22].

The asymptotic EP model was then applied to a multicellular model with irregularly shaped, closely spaced cells [23]. Overwhelmingly large numbers of pores are created in the PMs in response to a 20-kV/cm, 300-ns pulse, leading to spatially homogeneous EP. In contrast, a conventional 100-μs, 1-kV/cm EP pulse yields a spatially heterogeneous EP distribution.

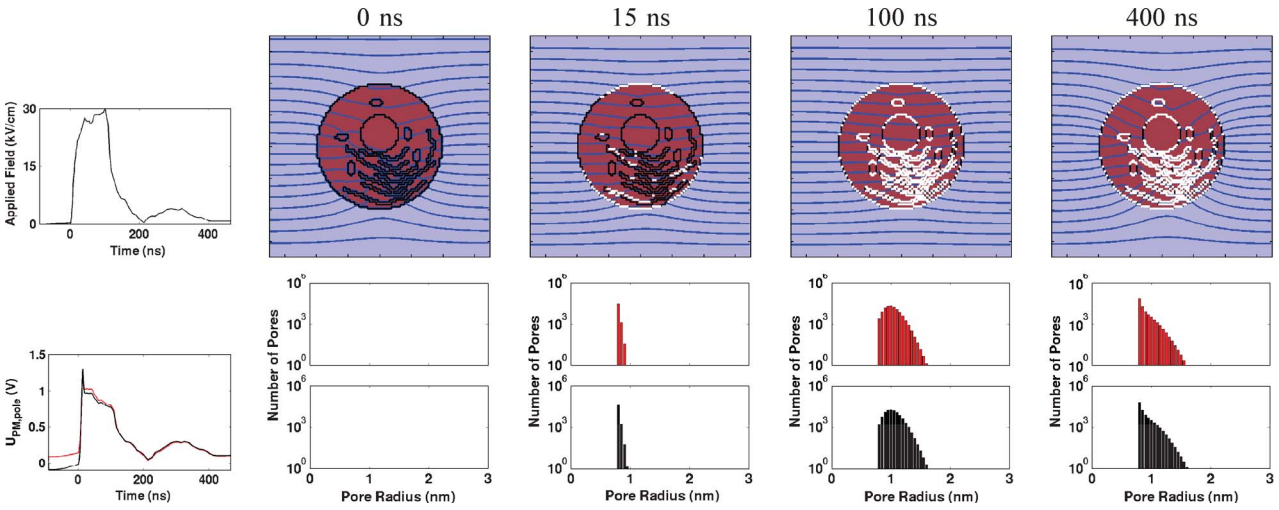

Fig. 5. *CTL model EP response of an isolated cell to a nsPEF pulse. A digitized experimental pulse waveform [29] is used with an isolated cell model [21], [24]. Upper left: Experimental pulse waveform (nominal 100-ns duration; the ~300-ns ragged tail contributes little to the highly nonlinear EP response). Lower left: Transmembrane voltage $U_m(t)$ at the anodic (red) and cathodic (black) poles of the circular cell. The spike following rapid charging is due to a creation burst of conducting small pores. Upper row of four panels: Spatial distributions of EP sites (white regions; $> 10^{13}$ pores/m^2) and equipotentials (black lines/curves; equipotentials of the response field of each panel are scaled separately). The top of the system model is an idealized (zero overvoltage) anode and the bottom is an idealized cathode, so that the applied field is uniform in the absence of the cell. Lower row of four top/bottom panel pairs: Red PM pore population histograms (bin width 0.05 nm) for the upper (anodic) side of the cell, with black histograms for the lower (cathodic) side. Note the semilogarithmic scale, showing that most pores are small (the minimum pore size; radius $r_p \approx 0.8$ nm at the peak, and falling off rapidly to one at $r_p \approx 1.6$ nm at the right most panel for both red and black distributions.*

C. CTL Models With Dynamic EP Models

The CTL method was extended to a dynamic pore membrane EP model (Fig. 1, right rectangle) for an isolated cell [21], [24]. The dynamic model was assigned to the PM and MOM while retaining the asymptotic model for the ER, NM, and MIM due to computational limitations. This feature increased the cell system model's complexity and realism which focuses on the PM and mitochondria (Fig. 5). Dynamic pores expand and contract in response to a pore energy landscape that itself depends on the local transmembrane voltage $U_{\mathrm{m}}(t)$ [25], [26]. Complex, spatially distributed voltage division occurs, involving both membranes and intervening aqueous regions. This means that different heterogeneous pore populations are created at different local membrane areas. The instantaneous distributions of pore sizes depends on both $U_{\mathrm{m}}(t)$ and also the history of the pore population (hysteresis is inescapable).

nsPEF and irreversible electroporation (IRE) have emerged as alternatives to conventional EP, motivated by potential clinical applications. Several papers reported nsPEF cell death by apoptosis rather necrosis [27]–[29]. This was a striking and provocative observation, as the intrinsic apoptotic pathway involves membranes of both the ER and mitochondria [19], [20]. In contrast, IRE pulses [30], [31] cause cell death by necrosis. Our single-cell models with dynamic EP membrane models show that similar progressive EP of organelles and significant PM pore expansion is expected for longer, somewhat smaller exponential pulses [21]. The model also showed that intracellular EP is complex, suggesting that both molecular transport through pores and voltage gating of organelle channels are possible mechanisms for intracellular effects for pulses longer than a microsecond. This implies that nsPEF should not be necessary for intracellular EP [21]. The organelle-containing single-cell model with dynamic EP membrane models showed that both nsPEF and IRE cause significant intracellular EP, but with different intracellular spatial distribution of EP sites [24]. Generally, nsPEF causes supra-EP, involving only small pores that allow transport of small ions and molecules. In contrast, IRE pulses lead to larger pores facilitating transport of larger molecules.

A multicellular system model (spatial scale 100 μm) with irregularly shaped liver cells with dynamic EP membrane model (Fig. 6) was also used to describe nsPEF and IRE pulse responses [24], [32], [33]. The model showed significant redistribution of fields and currents through the large number of PM pores in both cases. This demonstrated that nsPEF pulses create a large number of pores that do not expand beyond 1.2-nm radius [33] (Fig. 6). In contrast, the IRE pulses cause expansion of some membrane pores leading to the presence of both small and large pores [24], [32]. Although the pores are small in the case of an nsPEF pulse, the sheer number of them increases the average tissue conductance beyond that is achieved for a longer IRE pulse [33].

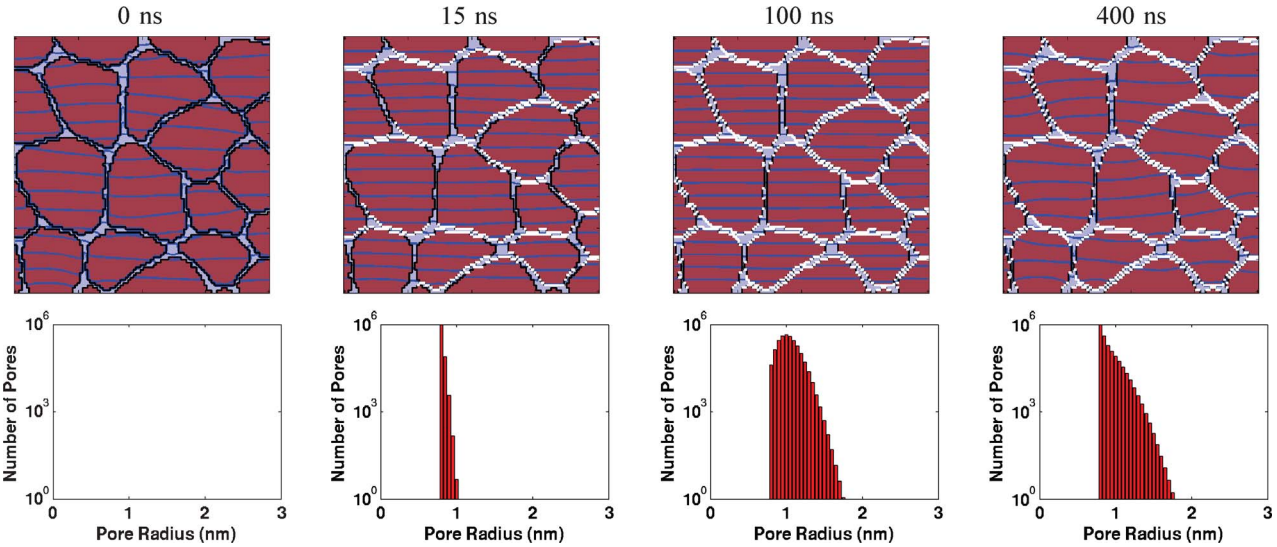

Fig. 6. *Multicellular CTL model response [24] to the nsPEF pulse of Fig. 5. Upper row of four panels: Spatial distribution of EP sites (white regions; $> 10^{13}$ pores/m^2) and equipotential curves/lines (dark blue). At the time designated $t = 0$ ns there is a small applied field (0.18 kV/cm) but neither the transmembrane voltages nor the time is sufficient to create pores in the irregularly shaped PMs. At $t = 15$ ns, pores have been created at many membrane sites, particularly those membranes that are parallel to the equipotentials (perpendicular to the applied field pulse). In contrast, there are some, but relatively few, at parts of the PMs that are nearly parallel to the field. The equipotentials are essentially parallel, so that within the in vivo environment (relatively little extracellular water) supra-electroporation is closer to being maximized. At $t = 100$ ns, many of the previously unporated PM regions now have pores, and the equipotentials remain nearly parallel (almost uniform field within the system). Finally, at $t = 400$ ns when the field pulse is greatly diminished but not zero, the porated sites remain unchanged, but the equipotentials are no longer parallel. This is consistent with decreased PM conductance (individual pore conductance is a function of U_m), due to partitioning associated with the Born energy [32], [33]). Lower row of four top/bottom panel pairs: The plots show the histogram of all membrane pores in the systems model (here all system PM pores). The membrane pores grow in size, but expand at most to about 1.8-nm radius, with the great majority having radii near 1 nm. Note that the leftmost panel appropriately has zero pores.*

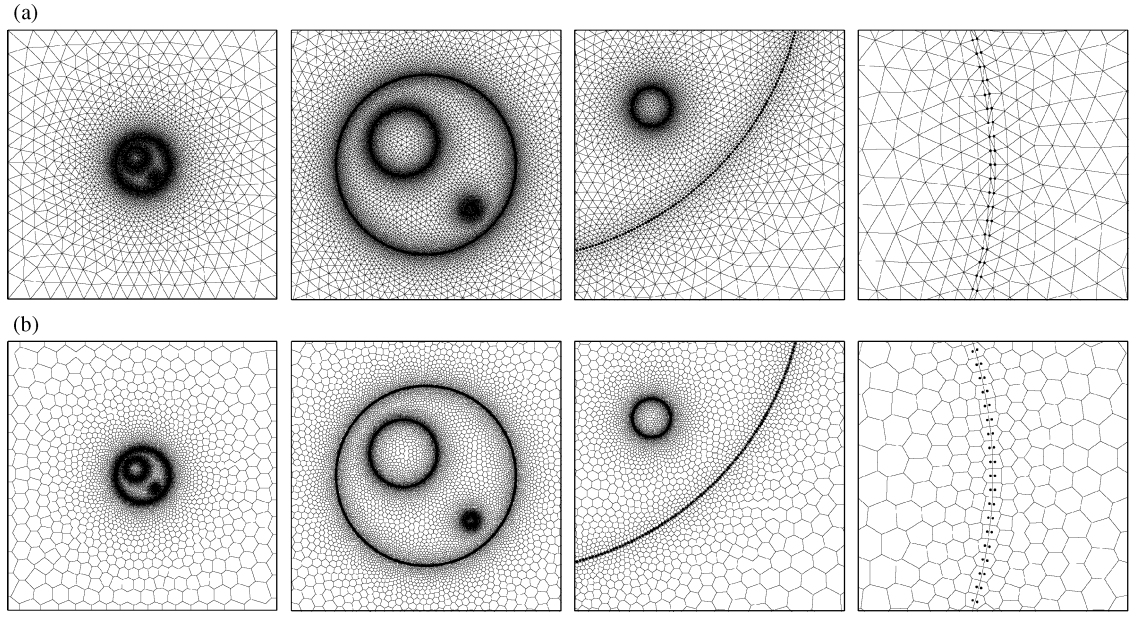

Fig. 7. *(a) MTN cell system mesh and (b) the associated Voronoi cells [34], each at three spatial scales (black dots indicate membrane-surface nodes). In the system model, there are 19 061 nodes, 38 061 triangles, and 44 691 edges. For a sense of scale, the lengths of the subfigure sides are (left to right) 80, 24, 7, and 0.3 μm. The spatial dynamic range varies from 80 μm (total system model) to 5 nm (membrane thickness), viz., about four orders of magnitude.*

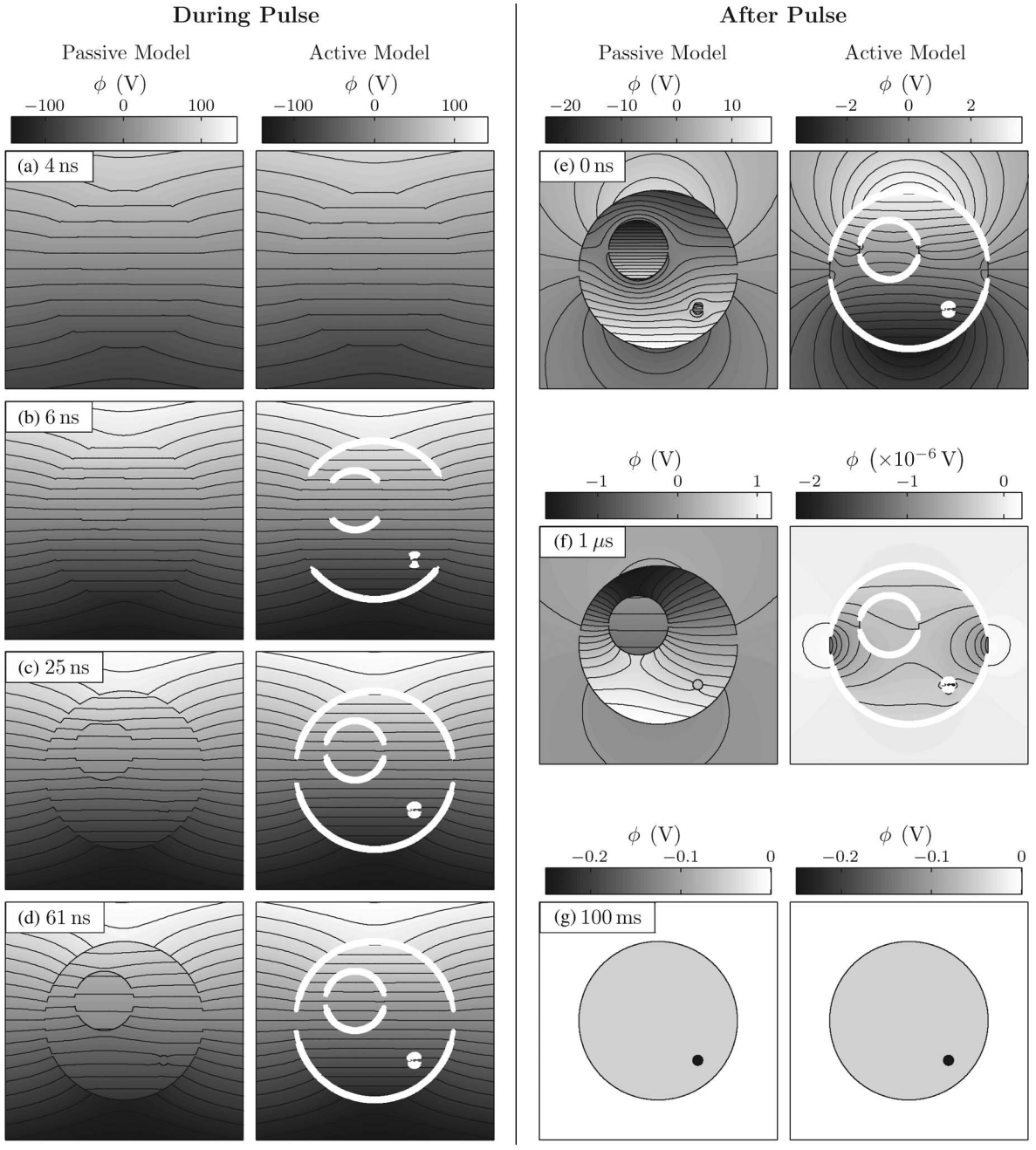

Fig. 8. *Passive and active cell system MTN model responses [34]. The waveform is an idealized (asymmetric trapezoid) version of an experimental 60-ns, 95-kV/cm pulse [45]. (a)–(d) Electric potential and pore density during the pulse for the passive (no EP; left) and active (right) versions of the cell system model. (e)–(g) Corresponding electrical and poration behavior after the pulse. For the active model with EP, pore density is indicated by the white line thickness (10^{14}, 10^{15}, 10^{16} m^{-2}). Twenty-one contour lines are uniformly spaced between the extreme values of their associated grayscale bars. Note that the intracellular and extracellular electric field magnitudes are not equal, even early in the pulse, because intracellular conductivity is one-fourth the extracellular conductivity. Here the pore lifetime is 3 ms, typical of pure lipid bilayer membranes [46]. The system model's temporal dynamic range involves short (10^{-9} s) to moderately long times (0.1 s), which covers eight orders of magnitude.*

D. MTN Models

An improved approach, an MTN, was also developed [7], and was described in a direct comparative study of the CTL and MTN methods [6]. With both better geometric representation and improved computational efficiency, and the asymptotic EP model (Fig. 2), this approach was used to create and solve a model of an idealized cell with two idealized, off-center organelles (Fig. 7) [34]. The large

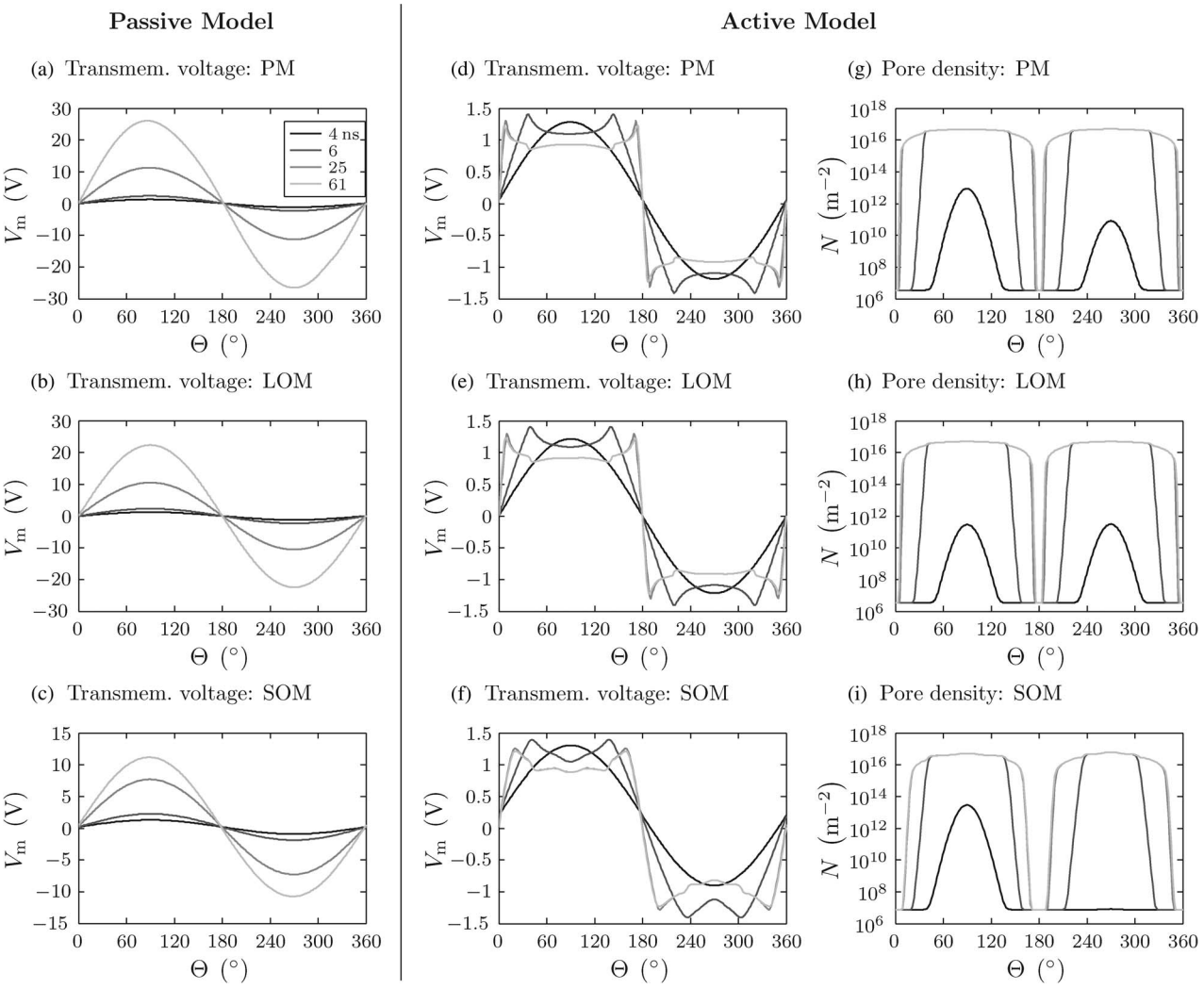

Fig. 9. ***Angular distributions of cell system MTN model responses [34]. (a)–(f) Transmembrane voltages and (g)–(i) pore density as a function of angle for the PM and also each idealized organelle membrane (LOM and SOM) for the passive and active cell models. Times are indicated by dark to light gray curves 4, 6, 25, and 61 ns. $\theta = 90^\circ$ is the anodic (positive) pole and $\theta = 270^\circ$ is the cathodic (negative) pole. Note that there are few changes in V_m and N between 25 and 61 ns. Consequently, the 61-ns traces often obscure the 25-ns traces. The flattening of voltage profiles by preferential creation of conducting pores near polar regions is a characteristic feature of EP [14], [15].***

organelle membrane (LOM) is typical of a cell's nucleus, and the small organelle membrane (SOM) has the approximate size of a mitochondrion. Both organelle models were based on single membranes for ease of interpretation, even though both the nuclear envelope and the mitochondrial membranes actually consist of two bilayer-based membranes (included in our other models).

The MTN model also demonstrated the complex electrical behavior of EP in both space and time, even though the relatively simple asymptotic membrane EP model was employed. Examples of the electrical response are shown in Fig. 8 (2-D equipotentials and white electroporation sites) and in Fig. 9 (angular distribution of the transmembrane voltage at four different times for the PM, LOM, and SOM).

The response of the model MTN [34] to an idealized 60-ns, 95-kV/cm pulse highlights the inadequacy of passive membrane models in describing the dynamic changes in membrane electrical properties caused by a large electric field (Fig. 8). The responses of the passive and active models are similar prior to the formation of membrane pores. As the polar regions of the PM and organelle membranes reach transmembrane voltages of 1–1.4 V, pores are rapidly formed causing a tremendous increase in membrane conductance. The MTN model also demonstrates the self-limiting nature of pore creation, as a large number of local pores decrease the transmembrane voltage to ~1 V causing the pore creation to slow. The passive model does not incorporate this dynamic, nonlinear change in membrane conductance.

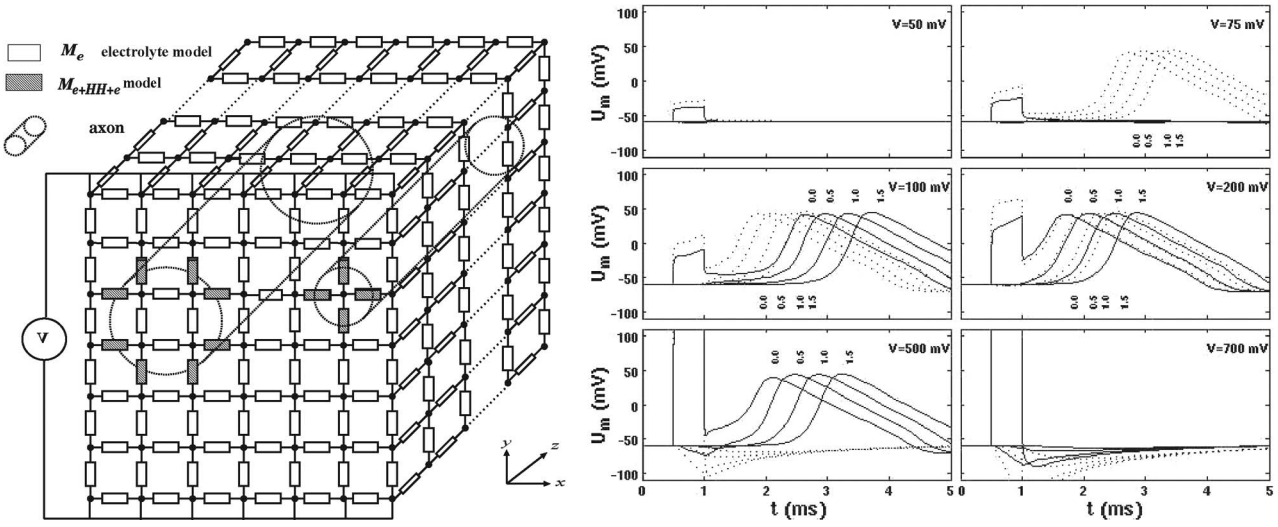

Fig. 10. *Two-axon transport lattice system model (left) and transmembrane voltage responses (right) [35]. The system model is a 3-D CTL with 7 × 7 × 25 nodes in the x-, y-, and z-directions (node separation of $\ell_x = \ell_y = 10$ μm in the x- and y-directions; $\ell_z = 100$ μm in the z-direction). Each local area of the axon membrane is represented by a Hodgkin–Huxley (HH) model that connects two aqueous electrolyte regions (intracellular and extracellular electrolyte). The many interconnected local electrolyte models allow fields and currents to approximately satisfy Laplace's equation within the extracellular region [4]. Note that we do not use Laplace's equation outside the cell, but instead rely on collective transport behavior of local aqueous region models to provide the response. This appears to work well, because both the distribution and the behavior of local models are similar to those of local populations of the channels and membrane regions of a real axon. Here the model's response is computed by solving the corresponding 3-D circuit using SPICE, which solves for the transient voltage at each node in response to an electrode pair voltage pulse. The two application electrodes are vertical lines of nodes on opposing sides of the volume at z = 0. A 0.5-ms square voltage pulse stimulus ranging from 50 to 1500 mV (top of each panel) was applied to the two idealized (zero overvoltage) electrodes located on the sides of the system model. Dotted plots are the responses of the larger axon; solid plots are the responses of the smaller axon. This and other results of the original paper [35] provide an example of nonlinear responses other than EP.*

Without it the transmembrane voltage reaches unrealistic values (over 20 V).

The active model shows that all membrane areas achieve significant pore densities except narrow equatorial bands of the PM, LOM, and SOM (Fig. 8). The asymptotic membrane EP model shows that the high conductance state of the membrane causes significant penetration of electric field into intracellular and intraorganellar spaces. In contrast, the low membrane conductance in the cell model with passive membrane model did not allow significant field penetration [34].

The angular profile of the active model response (Fig. 9) shows flattening in transmembrane voltage and pore density around the poles. These regions widen during the pulse. As pores form, the conductance of the membrane increases driving down the transmembrane voltage because of voltage division with the fixed conductance of the surrounding electrolyte. This dynamic behavior was shown to cause waves of elevated transmembrane voltage and pore creation traveling from the membrane poles toward the membrane equators [34].

E. CTL Nerve Models

Both one- and two-axon models were constructed in 3-D, using a coarsely discretized CTL (Fig. 10). The motivation is exploration of models that can accommodate external electrodes and multiple axons. After including a sigmoidal, ion channel population average conductance change due to local membrane voltage-gated channel models (functions), we demonstrated that action potential initiation and propagation can be incorporated [35]. The one-axon model behavior agrees reasonably with experiment. The two-axon model is more difficult to verify as (to our knowledge) no comparable experiments have been reported.

In the future, addition of explicit representations of nodes of Ranvier and myelinated sheath regions is anticipated, with saltatory (leaping) conduction between nodes due to increased nodes of Ranvier potentials due to greater insulation of intervening myelinated regions. Future models should also, therefore, contain the possibility of considering nonthermal myelinated nerve damage that has been reported for relatively small applied electric fields [36]. Space-filling models of nerves and nerve bundles offer the prospect of a better quantitative understanding of nonthermal damage due to electroporation of nerves.

F. CTL Heat Transport Models

Joule heating is an inescapable consequence of applying electric fields to biological systems. Extremes

range from cancer hyperthermia, tumor ablation, and some cases of electric shock injury, to very little heating for responses of very small fields (sharks and rays in the ocean). EP also involves heating, but the temperature rise is itself too small to cause significant pore formation. Heat transport at the tissue level is often described by the Penne's bioheat equation [37]. A CTL can also be used, and can involve complexity such as temperature-dependent perfusion [38]. While there are many existing modeling methods applicable to heat transfer, we suggest that in modeling the response of a biological system to electric fields by CTL or MTN, a geometrically identical lattice or network with 1-D heat transport models could be used simultaneously to describe estimates of spatially distributed temperature.

G. Molecular Transport in Tissue and Whole Body Models

In the case of significant but transient heating by microwaves (or EP) biologically active molecules can be released from cells [39]. The released solutes can then move within the interstitial space between cells, enter blood capillaries, and then be transported away from the release site by blood perfusion. For small solutes this is similar to the removal (clearance) of heat by the bioheat equation.

We have demonstrated the use of a 1-D transport lattice for this problem which shows how released solutes can be redistributed within the body via blood circulation, and eventually eliminated, e.g., by renal function [39]. This, in turn, suggests how cell level models within tissue could be combined with tissue clearance, and then coupled to well-established pharmacokinetics. In principle, this approach could be used with anatomically correct models of the whole human body [40], [41].

Intracellular release of calcium and other EP-related modeling has also been reported [47].

H. Future Directions

A recently completed MTN features several major improvements [8]. These features include simultaneous electrical, poration responses, and electrodiffusion of solutes both within aqueous compartments and through rapidly changing, heterogeneous pore populations in cell membranes due to EP.

Molecular dynamics (MD) simulations of EP involve very small ($\sim 10^{-14}$ m^{-2}) planar bilayer membranes. These require extremely large fields ($\sim$100 kV/cm or more) to yield pores on computationally feasible time scales ($\sim$10 to $\sim$100 ns) [42], [43]. Real cells have orders of magnitude more membrane area ($\sim 10^{-9}$ m^2); five orders of magnitude larger for the outer, PM. Cells are exposed to pulses ranging from $\sim$1 ns to almost 1 s (nine orders of magnitude), with most field pulse strengths 10 kV/cm or less, and durations usually 100 μs or longer. The spatial, temporal, and field magnitudes are thus very different for MD simulations and most cell EP, with overlap only for very short and extremely large pulse strengths. For comparison, we note that the fundamental attributes are: 1) MD has molecular scale realism for individual pore behavior, while continuum models of single pores appear increasingly wanting; and 2) the fundamental advantage of continuum cell system models are system level interactions and experimental realism. We note that both approaches use approximations.

We argue that neither MD nor cell level continuum approaches are likely to succeed in isolation. Instead, future developments should seek extraction of single pore behavior and properties from MD results that can be averaged and used in cell system models (many pores participate). Overall, the combination of theory-based models and quantitative experimental results should be central to long-term success in quantitatively understanding and developing EP applications.

Our models are motivated by the goal of approximate evaluation of combinations of pulses, molecules and cells, viz., understanding approximately, but usefully, the delivery or redistribution of biologically active molecules within different cellular systems. A library of cell system computer models that begins to be useful could be regarded as an early stage of creating an approximate analog to cell lines, which are widely used in biology, biotechnology, and new approaches to clinical medicine. Such modeling capability should be productivity enhancing, aiding interpretation of existing experiments, assisting future applications development, and possibly pointing to discoveries. ■

Acknowledgment

The authors would like to thank A. T. Esser, and R. S. Son for valuable discussions and K. G. Weaver for computer assistance.

REFERENCES

[1] J. C. Weaver, "Electroporation of biological membranes from multicellular to nano scales," *IEEE Trans. Dielectr. Electr. Insul.*, vol. 10, no. 5, pp. 754–768, Oct. 2003.

[2] E. Neumann and S. Kakorin, "Physical chemical theory of membrane electroporation and electrotransfer of biogenic agents," in *Advanced Electroporation Techniques in Biology and Medicine*, A. G. Pakhomov, D. Miklavčič, and M. S. Markov, Eds. Boca Raton, FL: CRC Press, 2010, pp. 3–18.

[3] A. S. Verkman, "Solute and macromolecule diffusion in cellular aqueous compartments," *TRENDS Biochem. Sci.*, vol. 27, pp. 27–33, 2002.

[4] J. C. Weaver and Y. A. Chizmadzhev, "Theory of electroporation: A review," *Bioelectrochem. Bioenergetics*, vol. 41, pp. 135–160, 1996.

[5] T. R. Gowrishankar and J. C. Weaver, "An approach to electrical modeling of single and multiple cells," *Proc. Nat. Acad. Sci.*, vol. 100, pp. 3203–3208, 2003.

[6] K. C. Smith, T. R. Gowrishankar, A. T. Esser, D. A. Stewart, and J. C. Weaver, "Spatially distributed, dynamic transmembrane voltages of organelle and cell membranes due to 10 ns pulses: Predictions of meshed and unmeshed transport network models," *IEEE Trans. Plasma Sci.*, vol. 34, no. 4, pt. 2, pp. 1394–1404, Aug. 2006.

[7] K. C. Smith, "Modeling cell and tissue electroporation," S.M. thesis, Dept. Electr.

Eng. Comput. Sci., Massachusetts Inst. Technol., Cambridge, MA, 2006.

[8] K. C. Smith, "A unified model of electroporation and molecular transport," Ph.D. dissertation, Massachusetts Inst. Technol., Harvard-MIT Div. Health Sci. Technol., Cambridge, MA, 2011.

[9] T. Kotnik and D. Miklavčič, "Second-order model of membrane electric field induced by alternating external electric fields," *IEEE Trans. Biomed. Eng.*, vol. 47, no. 8, pp. 1074–1081, Aug. 2000.

[10] D. A. Stewart, T. R. Gowrishankar, K. C. Smith, and J. C. Weaver, "Cylindrical cell membranes in uniform applied electric fields: Validation of a transport lattice method," *IEEE Trans. Biomed. Eng.*, vol. 52, no. 10, pp. 1643–1653, Oct. 2005.

[11] T. R. Gowrshankar, D. Stewart, and J. C. Weaver, "Model of a confined spherical cell in uniform and heterogeneous applied electric fields," *Bioelectrochemistry*, vol. 68, pp. 181–190, 2006.

[12] J. A. Lundqvist, F. Sahlin, M. A. Aberg, A. Stromberg, P. S. Eriksson, and O. Orwar, "Altering the biochemical state of individual cultured cells and organelles with ultramicroelectrodes," *Proc. Natl. Acad. Sci.*, vol. 95, pp. 10356–10360, 1998.

[13] M. Wang, O. Orwar, J. Olofsson, and S. G. Weber, "Single-cell electroporation," *Anal. Bioanal. Chem.*, vol. 397, pp. 3235–3248, 2010.

[14] K. A. DeBruin and W. Krassowska, "Modeling electroporation in a single cell: I. Effects of field strength and rest potential," *Biophys. J.*, vol. 77, pp. 1213–1224, 1999.

[15] K. A. DeBruin and W. Krassowska, "Modeling electroporation in a single cell: II. Effects of ionic concentration," *Biophys. J.*, vol. 77, pp. 1225–1233, 1999.

[16] J. C. Neu and W. Krassowska, "Asymptotic model of electroporation," *Phys. Rev. E*, vol. 59, pp. 3471–3482, 1999.

[17] D. A. Stewart, T. R. Gowrishankar, and J. C. Weaver, "Transport lattice approach to describing cell electroporation: Use of a local asymptotic model," *IEEE Trans. Plasma Sci.*, vol. 32, no. 4, pt. 2, pp. 1696–1708, Aug. 2004.

[18] T. R. Gowrishankar, A. T. Esser, Z. Vasilkoski, K. C. Smith, and J. C. Weaver, "Microdosimetry for conventional and supra-electroporation in cells with organelles," *Biochem. Biophys. Res. Commun.*, vol. 341, pp. 1266–1276, 2006.

[19] G. Kroemer, L. Galluzzi, and C. Brenner, "Mitochondrial membrane permeabilization in cell death," *Physiol. Rev.*, vol. 87, pp. 99–163, 2007.

[20] Y.-L. P. Ow, D. R. Green, Z. Hao, and T. W. Mak, "Cytochrome c: Functions beyond respiration," *Nat. Rev. Mol. Cell Biol.*, vol. 9, pp. 532–524, 2008.

[21] A. T. Esser, K. C. Smith, T. R. Gowrishankar, Z. Vasilkoski, and J. C. Weaver, "Mechanisms for the intracellular manipulation of organelles by conventional electroporation," *Biophys. J.*, vol. 98, pp. 2506–2514, 2010.

[22] K. H. Schoenbach, S. J. Beebe, and E. S. Buescher, "Intracellular effect of ultrashort pulses," *Bioelectromagnetics*, vol. 22, pp. 440–448, 2001.

[23] T. R. Gowrishankar and J. C. Weaver, "Electrical behavior and pore accumulation in a multicellular model for conventional and supra-electroporation," *Biochem. Biophys. Res. Commun.*, vol. 349, pp. 643–653, 2006.

[24] T. R. Gowrishankar, A. T. Esser, K. C. Smith, R. S. Son, and J. C. Weaver, "Intracellular electroporation site distributions: Modeling examples for nsPEF and IRE pulse waveforms," in *Proc. 33rd Annu. Int. Conf. IEEE Eng. Med. Biol. Soc.*, Boston, MA, 2011, pp. 732–735.

[25] A. Barnett and J. C. Weaver, "Electroporation: A unified, quantitative theory of reversible electrical breakdown and rupture," *Bioelectrochem. Bioenergetics*, vol. 25, pp. 163–182, 1991.

[26] S. A. Freeman, M. A. Wang, and J. C. Weaver, "Theory of electroporation for a planar bilayer membrane: Predictions of the fractional aqueous area, change in capacitance and pore-pore separation," *Biophys. J.*, vol. 67, pp. 42–56, 1994.

[27] S. J. Beebe, P. M. Fox, L. J. Rec, K. Somers, R. H. Stark, and K. H. Schoenbach, "Nanosecond pulsed electric field (nsPEF) effects on cells and tissues: Apoptosis induction and tumor growth inhibition," *IEEE Trans. Plasma Sci.*, vol. 30, no. 1, pt. 2, pp. 286–292, Feb. 2002.

[28] E. B. Garon, D. Sawcer, P. T. Vernier, T. Tang, Y. Sun, L. Marcu, M. A. Gundersen, and H. P. Koeffler, "In vitro and in vivo and a case report of intense nanosecond pulsed electric fields as a local therapy for human malignancies," *Int. J. Cancer*, vol. 121, pp. 675–682, 2007.

[29] R. Nuccitelli, K. Tran, S. Sheikh, B. Athos, M. Kreis, and P. Nuccitelli, "Optimized nanosecond pulsed electric field therapy can cause murine malignant melanomas to self-destruct with a single treatment," *Int. J. Cancer*, vol. 127, pp. 1727–1736, 2010.

[30] L. Miller, J. Leor, and B. Rubinsky, "Cancer cells ablation with irreversible electroporation," *Technol. Cancer Res. Treatment*, vol. 4, pp. 699–705, 2005.

[31] B. Rubinsky, "Irreversible electroporation in medicine," *Technol. Cancer Res. Treatment*, vol. 6, pp. 255–159, 2007.

[32] A. T. Esser, K. C. Smith, T. R. Gowrishankar, and J. C. Weaver, "Towards solid tumor treatment by irreversible electroporation: Intrinsic redistribution of fields and currents in tissue," *Technol. Cancer Res. Treatment*, vol. 6, pp. 261–273, 2007.

[33] A. T. Esser, K. C. Smith, T. R. Gowrishankar, and J. C. Weaver, "Towards solid tumor treatment by nanosecond pulsed electric fields," *Technol. Cancer Res. Treatment*, vol. 8, pp. 289–306, 2009.

[34] K. C. Smith and J. C. Weaver, "Active mechanisms are needed to describe cell responses to submicrosecond, megavolt-per-meter pulses: Cell models for ultrashort pulses," *Biophys. J.*, vol. 95, pp. 1547–1563, 2008.

[35] D. A. Stewart, T. R. Gowrishankar, and J. C. Weaver, "Three dimensional transport lattice model for describing action potentials in axons stimulated by external electrodes," *Bioelectrochemistry*, vol. 69, pp. 88–93, 2006.

[36] G. S. Abramov, M. Bier, M. Capelli-Schellpfeffer, and R. C. Lee, "Alteration in sensory nerve function following electrical shock," *Burns*, vol. 22, pp. 602–606, 1996.

[37] H. Pennes, "Analysis of tissue and arterial blood temperatures in the resting human forearm," *J. Appl. Physiol.*, vol. 1, pp. 93–122, 1948.

[38] T. R. Gowrishankar, D. A. Stewart, G. T. Martin, and J. C. Weaver, "Transport lattice models of heat transport in skin with spatially heterogeneous, temperature-dependent perfusion," *Biomed. Eng. Online*, vol. 3, 2004, DOI: 10.1186/1475-925X-3-42.

[39] D. A. Stewart, T. R. Gowrishankar, and J. C. Weaver, "Skin heating and injury by prolonged millimeter wave exposure: Theory based on a skin model coupled to a whole body model and local biochemical release from cells at supraphysiologic temperatures," *IEEE Trans. Plasma Sci.*, vol. 34, no. 4, pt. 2, pp. 1480–1493, Aug. 2006.

[40] T. Nagaoka, E. Kunieda, and S. Watanabe, "Proportion-corrected scaled voxel models for Japanese children and their application to the numerical dosimetry of specific absorption rate for frequencies from 30 MHz to 3 GHz," *Phys. Med. Biol.*, vol. 53, no. 23, pp. 6695–6711, 2008.

[41] A. Christ, W. Kainz, E. G. Hahn, K. Honegger, M. Zefferer, E. Neufeld, W. Rascher, R. Janka, W. Bautz, J. Chen, B. Kiefer, P. Schmitt, H.-P. Hollenbach, J. Shen, M. Oberle, D. Szczerba, A. Kam, J. W. Guag, and N. Kuster, "The 'virtual family' project–Development of anatomical whole-body models of two adults and two children," *Comput. Med. Biol.*, vol. 55, pp. 23–38, 2010.

[42] A. A. Gurtovenko, J. Anwar, and I. Vattulainen, "Defect-mediated trafficking across cell membranes: Insights from in silico modeling," *Chem. Rev.*, vol. 110, pp. 6077–6103, 2010.

[43] P. T. Vernier, Z. A. Levine, and M. A. Gundersen, "Water bridges in electropermeabilized phospholipid bilayers," *Proc. IEEE*, submitted for publication.

[44] G. Kron, "Numerical solution of ordinary and partial differential equations by means of equivalent circuits," *J. Appl. Phys.*, vol. 16, pp. 172–186, 1945.

[45] W. Frey, J. A. White, R. O. Price, P. F. Blackmore, R. P. Joshi, R. Nuccitelli, S. J. Beebe, K. H. Schoenbach, and J. F. Kolb, "Plasma membrane voltage changes during nanosecond pulsed electric field exposures," *Biophys. J.*, vol. 90, pp. 3608–3615, 2006.

[46] K. C. Melikov, V. A. Frolov, A. Shcherbakov, A. V. Samsonov, Y. A. Chizmadzhev, and L. V. Chernomordik, "Voltage-induced nonconductive pre-pores and metastable pores in unmodified planar bilayer," *Biophys. J.*, vol. 80, pp. 1829–1836, 2001.

[47] P. T. Joshi and K. H. Shoenbach, "Bioelectric effects of intense ultrashort pulses," *Crit. Rev. Biomed. Eng.*, vol. 38, pp. 255–304, 2010.

ABOUT THE AUTHORS

Thiruvallur R. Gowrishankar received the Ph.D. degree in medical physics from the University of Chicago, Chicago, IL, in 1997.

He is currently a Research Scientist in Harvard-MIT Division of Health Sciences and Technology, Massachusetts Institute of Technology, Cambridge. His research interests include bioelectric phenomena, drug delivery, and medical devices.

Kyle C. Smith received the B.S.E. degree in biomedical engineering from Duke University, Durham, NC, in 2003, the S.M. degree in electrical engineering and computer science from the Massachusetts Institute of Technology, Cambridge, in 2006, and the Ph.D. degree in biomedical and electrical engineering from the Harvard-MIT Division of Health Sciences and Technology in 2011.

He is currently a Senior Research Scientist in the Center for Engineering and Medicine, Massachusetts General Hospital, Boston, MA, where he is developing novel microfluidic systems for capturing circulating tumor cells. His primary research interest is medical and diagnostic device technologies.

James C. Weaver, photograph and biography not available at the time of publication.